Dynamic characteristics of 410 nm semipolar $(20\bar{2}\bar{1})$ III-nitride laser diodes with a modulation bandwidth of over 5 GHz

Changmin Lee, Chong Zhang, Daniel L. Becerra, Seunggeun Lee, Charles A. Forman, Sang Ho Oh, Robert M. Farrell, James S. Speck, Shuji Nakamura, John E. Bowers, and Steven P. DenBaars

Citation: Appl. Phys. Lett. **109**, 101104 (2016); doi: 10.1063/1.4962430
View online: http://dx.doi.org/10.1063/1.4962430
View Table of Contents: http://aip.scitation.org/toc/apl/109/10
Published by the American Institute of Physics

APPLIED PHYSICS LETTERS **109**, 101104 (2016)

Dynamic characteristics of 410 nm semipolar $(20\bar{2}\bar{1})$ III-nitride laser diodes with a modulation bandwidth of over 5 GHz

Changmin Lee,[1,a)] Chong Zhang,[2] Daniel L. Becerra,[1] Seunggeun Lee,[2] Charles A. Forman,[1] Sang Ho Oh,[2] Robert M. Farrell,[1] James S. Speck,[1] Shuji Nakamura,[1,2] John E. Bowers,[1,2] and Steven P. DenBaars[1,2]

[1]*Materials Department, University of California, Santa Barbara, California 93106, USA*
[2]*Department of Electrical and Computer Engineering, University of California, Santa Barbara, California 93106, USA*

(Received 15 June 2016; accepted 19 August 2016; published online 8 September 2016)

The dynamic characteristics of III-nitride multi-quantum well laser diodes (LDs) emitting at 410 nm were investigated. LDs were grown on semipolar $(20\bar{2}\bar{1})$ bulk GaN substrates and fabricated into devices with cavity lengths ranging from 900 nm to 1800 nm. A 3-dB bandwidth of 5 GHz and 5 Gbit/s direct modulation with on-off keying were demonstrated, which were limited by the bandwidth of the photodetector used for the measurements. The differential gain of the LDs was determined to be $2.5 \pm 0.5 \times 10^{-16}\,cm^2$ by comparing the slope efficiency for different cavity lengths. Analysis of the frequency response showed that the *K*-factor, the gain compression factor, and the intrinsic maximum bandwidth were 0.33 ns, $7.4 \times 10^{-17}\,cm^3$, and 27 GHz, respectively. *Published by AIP Publishing.* [http://dx.doi.org/10.1063/1.4962430]

III-nitride laser diodes (LDs) were first demonstrated in 1996 and have been developed for high-power applications such as optical storage, medical, and solid-state lighting.[1] However, the performance of LDs grown on conventional polar (0001) *c*-plane GaN has been hindered due to polarization-induced electric fields, leading to a reduction of wave-function overlap.[2,3] Recent progress on semipolar and nonpolar planes has shown significant improvement in high-power performance of light emitting diodes (LEDs) and LDs by reducing the polarization-induced electric field.[4–12] In addition, semipolar and nonpolar LDs are expected to have higher optical gain than *c*-plane LDs due to a higher wave-function overlap and a reduction in the density of states.[13–15]

While conventional III-nitride LEDs have typical bandwidth limits in the MHz range,[16,17] recent studies on LDs for light fidelity (LiFi) applications have demonstrated more than 2.6 GHz bandwidth and 4 Gbit/s data transmission rate using a blue LD alone as well as 2 Gbit/s data transmission rate using a blue LD with a phosphor by on-off keying (OOK).[18,19] Higher order modulation schemes could have improved data rates.[20–23] Future LiFi applications will require high-power and high-efficiency solid-state light sources with a capacity for high-speed data transmission.[24] Since semipolar and nonpolar LDs are expected to have higher differential gain than *c*-plane LDs, they also have the potential for improvements in modulation bandwidth. Although blue LEDs and LDs are typically used as the excitation source for solid-state lighting systems, violet LEDs and LDs have potential candidates in high quality white lighting with red-green-blue phosphors. In addition, violet LDs may have advantages in terms of LiFi system performance due to potential challenges with creating high-speed photodetectors (PDs) that absorb light in the blue region of the spectrum.[25–27] In this letter, we study the dynamic characteristics and high-speed performance of violet semipolar III-nitride LDs for LiFi applications.

Violet LDs were grown on free standing bulk GaN semipolar $(20\bar{2}\bar{1})$ substrates by metalorganic chemical vapor deposition (MOCVD). As shown in Fig. 1(a), the epitaxial structure consisted of a 1 μm Si-doped *n*-GaN cladding layer, a 500 nm n^+-GaN topside contact layer ($[Si] = 5.2 \times 10^{19}\,cm^{-3}$), a 350 nm *n*-GaN buffer layer ($[Si] = 6.2 \times 10^{18}\,cm^{-3}$) to minimize the absorption loss, and a 60 nm composition graded n-$In_{0.025}Ga_{0.975}N$ waveguiding layer. The active region consisted of a 4 period undoped $In_{0.1}Ga_{0.9}N/GaN$ (3.5 nm/7 nm) multiple quantum well (MQW) structure, followed by a 16 nm p-$Al_{0.18}Ga_{0.82}N$ electron blocking layer (EBL) linearly graded in composition and doping down to GaN at the topside. Then, a 60 nm composition graded p-$In_{0.025}Ga_{0.975}N$ waveguiding layer and a 600 nm thick Mg-doped *p*-GaN cladding layer

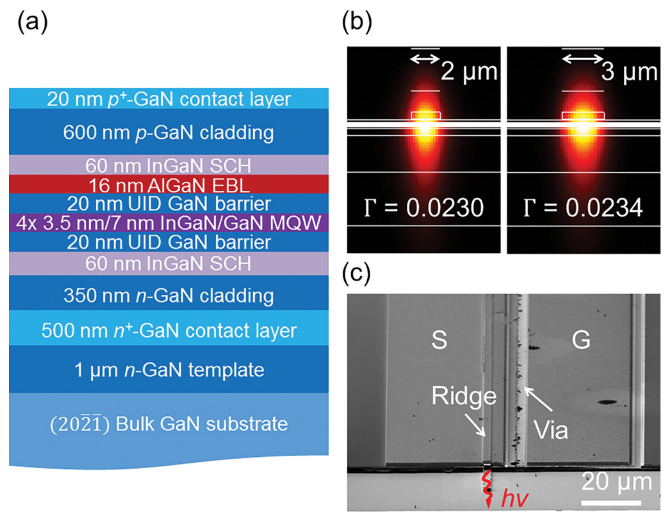

FIG. 1. (a) Schematic of the epitaxial structure of the LD on a $(20\bar{2}\bar{1})$ substrate. (b) Calculated optical mode for waveguide widths of 2 μm and 3 μm. (c) SEM image of the LD with ground-signal (GS) probe pads.

[a)]Author to whom correspondence should be addressed. Electronic mail: changminlee86@gmail.com

were grown followed by a 10 nm highly Mg-doped p^+-GaN contact layer.[28] The doping level of the n-GaN contact layer was optimized to obtain a low resistance topside n-type contact, which is essential for reducing the resistance of the device as well as enabling radio frequency (RF) measurements with ground-signal (GS) or ground-signal-ground (GSG) probe configurations.

After the MOCVD growth, the samples were fabricated into ridge waveguide LDs. Ridges with widths of 2 μm and 3 μm were formed by reactive ion etching (RIE). A commercial 2-D mode solver FIMMWAVE[29] was used to model the waveguide of the 2 μm and 3 μm LD and calculate a confinement factor of 0.0230 and 0.0234, respectively, as shown in Fig. 1(b). 200 nm of SiO_2 was deposited as a passivation layer onto the field and ridge sidewalls via sputtering and was lifted off of the laser ridges using a self-aligned process.[8] After wet etching a portion of the SiO_2 layer, the window for n-via contact area was etched via RIE down to the center of a 500-nm n^+-GaN layer to form the topside n-type contact. Ti/Al/Ni/Au (15/100/100/100 nm) n-contacts were deposited by electron beam evaporation, followed by rapid thermal annealing (RTA) with N_2 ambient at 450 °C to lower the contact resistance. Pd/Au (30/100 nm) p-contacts were deposited on top of the ridges, followed by common pad metals of Ti/Au (15/1000 nm) for both p- and n-pads. Mirror facets were formed by RIE and were left uncoated. The cavity lengths of the LDs ranged from 900 μm to 1800 μm. Figure 1(c) shows a scanning electron microscopy image of a 2 μm LD with a topside n-contact.

The light-current-voltage (L-I-V) characteristics of the LD with the highest bandwidth (2 μm wide and 1200 μm long) were measured under continuous wave (CW) operation at 15 °C, as shown in Fig. 2(a). The threshold current (I_{th}) and threshold current density (J_{th}) were 150 mA and 6.25 kA/cm^2, respectively, with a corresponding threshold voltage (V_{th}) of 5.1 V using a four-probe measurement. The slope efficiency and differential efficiency were 0.35 W/A and 23%, respectively, with etched facets before high-reflection coating. An injection efficiency of 80% was extracted by analyzing the dependence of differential efficiency on cavity length for a number of different LDs, which is in a good agreement with the data reported by Becerra *et al.*[11] The internal loss was estimated to be 16.9 cm^{-1} by considering the lowered reflectivity of the RIE-etched facet.[30] The lasing wavelength was around 410 nm, as shown in Fig. 2(b).

The small signal modulation characteristics can be derived from the carrier and photon density rate equations[31]

$$\frac{dn}{dt} = \frac{\eta_i I}{qV} - \frac{n}{\tau} - \upsilon_g\left(g_{th} + \frac{dg}{dn}\Delta n\right)s, \tag{1}$$

$$\frac{ds}{dt} = \Gamma \upsilon_g\left(g_{th} + \frac{dg}{dn}\Delta n\right)s - \frac{s}{\tau_p}, \tag{2}$$

where n and s are the carrier and photon densities in the active region, respectively, η_i is the injection efficiency, I is the drive current, q is the electron charge, V is the volume of the active layer, τ and τ_p are the carrier and photon (or cavity) lifetimes, respectively, υ_g is the group velocity, Γ is the optical confinement factor, and g_{th} is the threshold material gain. Under small signal conditions, a small fluctuation of

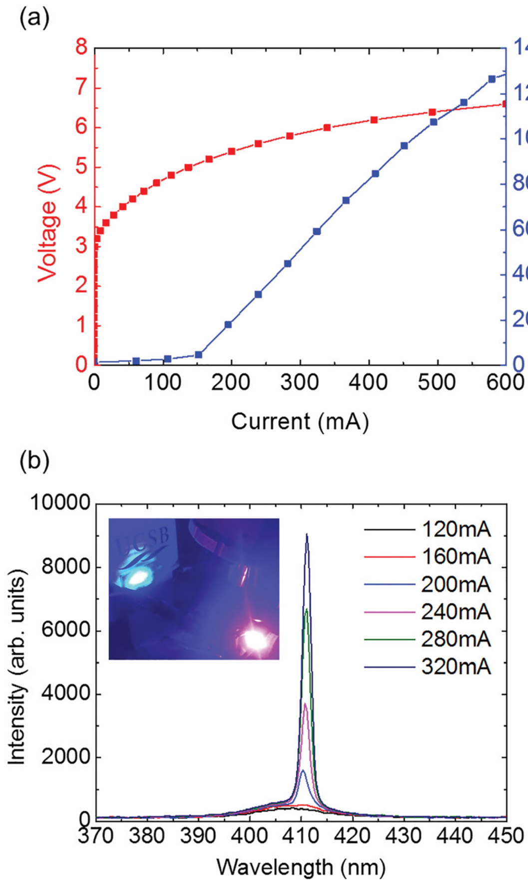

FIG. 2. (a) CW L-I-V characteristic for a 2 μm $\times$ 1200 μm LD measured with a 4 point probe configuration. (b) Electroluminescence spectra for different drive currents for the same LD. Inset: far field pattern of emission from the laser.

gain is added onto the threshold gain by multiplying the differential gain, dg/dn, by the fluctuation in carrier density, Δn. The spontaneous emission that is coupled into the lasing mode is ignored far above the threshold for this modulation condition. The small signal modulation for both carriers and photons is proportional to a second-order transfer function[31]

$$H(\omega) = \frac{\omega_R^2}{\omega_R^2 + \omega^2 + j\omega\gamma}, \tag{3}$$

where ω_R is the relaxation resonance frequency (or $f_R = \omega_R/2\pi$) and γ is the damping factor.

The sinusoidal small signal modulation was performed with an Agilent E8361A PNA network analyzer and received at an ALPHALAS UPD-50-UP high-speed Si p-i-n photodetector (PD). The bandwidth of the PD was measured with a 410 nm pulse train by frequency doubling a mode locked Ti-Sapphire laser emitting at 820 nm.[32] The measured bandwidth of the PD was 3.76 GHz as shown in Fig. 3(a). As shown in Fig. 3(b), the small-signal frequency response of the 2 μm wide by 1200 μm long LD was recovered by subtracting the fitted PD response, although the resonance peaks were still saturated near 4 GHz. The highest measured 3-dB bandwidth of the LD was 5 GHz at 220 mA of drive current, which was limited by the bandwidth of the PD. This can be concluded because the data before subtracting the PD response hit the noise floor near 4.8 GHz. It should be possible to obtain higher

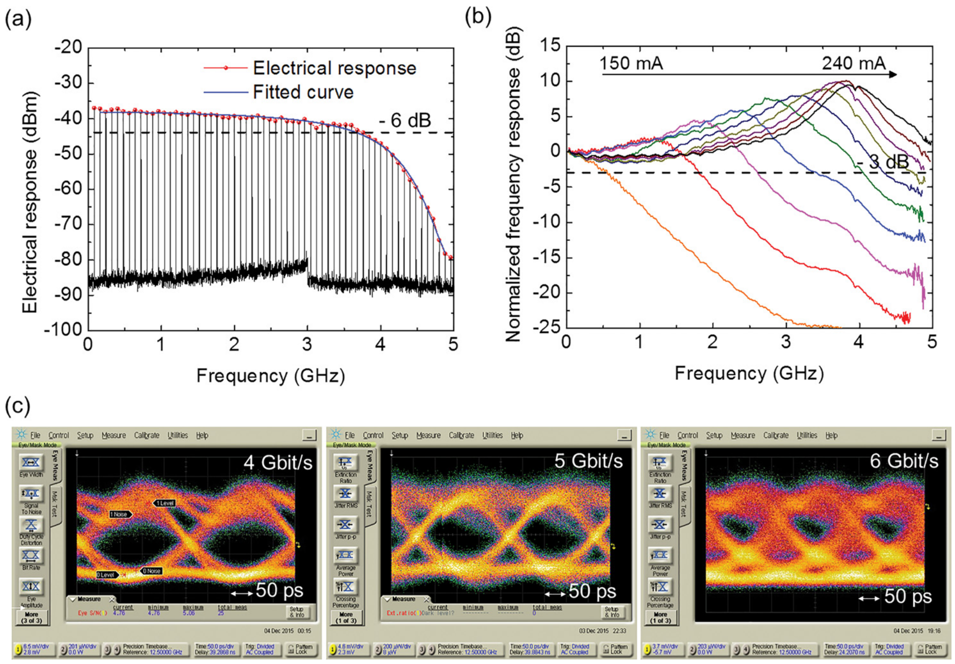

FIG. 3. (a) Frequency response of a Si *p-i-n* PD measured with a femtosecond pulsed Ti-Sapphire mode locked laser. (b) Small signal frequency response of $2\,\mu m \times 1200\,\mu m$ LD at different drive currents with 10 mA increment. (c) Eye diagrams for 4 Gbit/s, 5 Gbit/s, and 6 Gbit/s NRZ OOK modulation of the LD.

3-dB bandwidths with a higher speed PD that covers the UV-violet spectrum because the LD bandwidth is not the limiting component in the experimental setup.

Large signal modulation was performed to evaluate the capability of the LD for data transmission. The LD was driven by using a $2^{31} - 1$ non return-to-zero (NRZ) OOK pseudorandom bit sequence (PRBS) with a peak-peak 1.5 V drive input signal. The best optimized open eye diagram was obtained at 280 mA of drive current up to 4 Gbit/s with a 4.76 of signal-to-noise (SNR) ratio, as shown in Fig. 3(c). The highest data rate with a clearly open eye diagram was 5 Gbit/s, while 6 Gbit/s was limited by the bandwidth of PD.

To investigate the intrinsic modulation capability of the LDs, the differential gain, $\partial g/\partial n$, can be derived by the following equation for f_R:

$$f_R = \frac{1}{2\pi}\left[\frac{\Gamma v_g \dfrac{dg}{dn}}{qV}\eta_i(I - I_{th})\right]^{1/2}. \tag{4}$$

Figure 4(a) shows the dependence of relaxation resonance frequency on the drive current for different cavity sizes. The slopes of the curves were highly dependent on each cavity size, resulting in similar differential gains as expected. The slopes ranged from 0.5543 GHz/mA$^{1/2}$ for the largest cavity to 0.2646 GHz/mA$^{1/2}$ for the smallest cavity. The differential gains ranged from 1.94×10^{-16} cm^2 for the largest cavity to 2.84×10^{-16} cm^2 for the smallest cavity, as shown in Fig. 4(b). These values are in a good agreement with the reported differential gains of other III-nitride QW LDs and even comparable with those of quantum dot (QD) and nanowire (NW) LDs.[33–37] Compared to conventional polar *c*-plane LDs, the differential gain of semipolar $(20\bar{2}\bar{1})$ LDs is expected to be higher due to the higher electron-hole wave-function overlap in the lower density of states.[13,38,39] At low power operation, where gain compression is not significant, high differential gain leads to a higher f_R, resulting in a higher modulation bandwidth.[40]

For high power operation, where gain compression is significant, the modulation bandwidth depends more on the damping factor (or *K*-factor) than f_R.[31] As shown in Fig. 5, the *K*-factors were obtained by fitting the measured damping factor and f_R with the following relationship:

$$\gamma = K f_R^2 + \gamma_0, \tag{5}$$

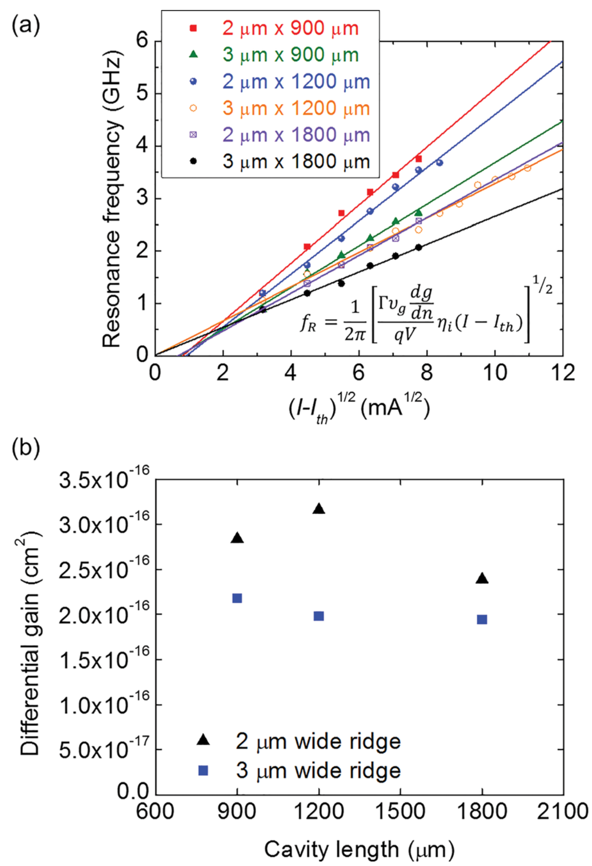

FIG. 4. (a) Dependence of relaxation resonance frequency on $(I-I_{th})^{1/2}$, where I is the drive current and I_{th} is threshold current. (b) Dependence of differential gain on cavity size.

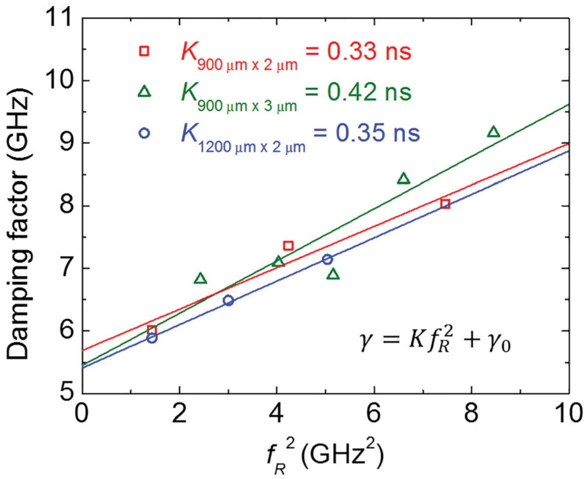

FIG. 5. Dependence of the damping factor on the square of the resonance frequency ($f_R{}^2$) for the three smallest devices with the lowest K-factors.

where γ_0 is the damping factor offset. Since parasitic roll-off of larger cavities occurs at lower frequencies, the smallest three cavities were analyzed at low injection levels and found to be in a good agreement. The lowest K-factor and the corresponding damping factor offset were 0.33 ns and 5.69 GHz for the 2 μm wide by 900 μm long LD, respectively. The gain compression factor was calculated to be 7.4×10^{-17} cm^3 by $K = 4\pi^2\tau_p(1 + \varepsilon\Gamma g_{th}/(dg/dn))$, where ε is the gain compression factor.[31] The intrinsic maximum bandwidth can be also obtained by the K-factor, which is the bandwidth limit due to the photon lifetime of the cavity. The maximum bandwidth occurs when the 3-dB bandwidth is at the resonance frequency. Hence, the calculated intrinsic maximum bandwidth was 27 GHz by $f_{3dB}^{max} = \sqrt{2}(2\pi/K)$, where $(\gamma/\omega_R)^2 = -3$ dB, in Eq. (3).

In summary, the dynamic characteristics of CW violet III-nitride LDs grown on the semipolar $(20\bar{2}\bar{1})$ plane were studied. A 3-dB bandwidth of 5 GHz was achieved giving an open eye diagram for a data rate of 5 Gbit/s. The differential gain of the LDs was determined to be $2.5 \pm 0.5 \times 10^{-16}$ cm^2 by comparing the slope efficiency for different cavity lengths. The calculated K-factor, the gain compression factor, and the intrinsic maximum bandwidth were 0.33 ns, 7.4×10^{-17} cm^3, and 27 GHz, respectively. Although the measured bandwidth was limited by the PD, these results show the potential of III-nitride semipolar LDs for high-speed visible light communication.

This work was funded by the KACST-KAUST-UCSB Solid State Lighting Program (SSLP) and by the Solid State Lighting and Energy Electronics Center (SSLEEC) at University of California, Santa Barbara (UCSB). A portion of this work was done in the UCSB nanofabrication facility, part of the National Science Foundation (NSF) funded Nanotechnology Infrastructure Network (NNIN) (ECS-0335765). This work also made use of UCSB Materials Research Laboratory (MRL) central facilities supported by the NSF MRSEC Program (DMR05-20415). The authors thank Professor L. A. Coldren for fruitful discussions.

[1]S. Nakamura, M. Senoh, S. Nagahama, N. Iwasa, T. Yamada, T. Matsushita, H. Kiyoku, and Y. Sugimoto, Jpn. J. Appl. Phys., Part 2 **35**, L74 (1996).
[2]J. S. Speck and S. F. Chichibu, MRS Bull. **34**, 304 (2009).
[3]H. Masui, J. Sonoda, N. Pfaff, I. Koslow, S. Nakamura, and S. P. DenBaars, J. Phys. D: Appl. Phys. **41**, 165105 (2008).
[4]S. P. DenBaars, D. Feezell, K. Kelchner, S. Pimputkar, C.-C. Pan, C.-C. Yen, S. Tanaka, Y. Zhao, N. Pfaff, R. Farrell, M. Iza, S. Keller, U. Mishra, J. S. Speck, and S. Nakamura, Acta Mater. **61**, 945 (2013).
[5]D. F. Feezell, J. S. Speck, S. P. Denbaars, and S. Nakamura, J. Disp. Technol. **9**, 190 (2013).
[6]D. F. Feezell, M. C. Schmidt, S. P. Denbaars, and S. Nakamura, MRS Bull. **34**, 318 (2009).
[7]R. M. Farrell, D. F. Feezell, M. C. Schmidt, D. A. Haeger, K. M. Kelchner, K. Iso, H. Yamada, M. Saito, K. Fujito, D. A. Cohen, J. S. Speck, S. P. DenBaars, and S. Nakamura, Jpn. J. Appl. Phys., Part 2 **46**, L761 (2007).
[8]R. M. Farrell, P. S. Hsu, D. A. Haeger, K. Fujito, S. P. DenBaars, J. S. Speck, and S. Nakamura, Appl. Phys. Lett. **96**, 231113 (2010).
[9]A. Pourhashemi, R. M. Farrell, M. T. Hardy, P. S. Hsu, K. M. Kelchner, J. S. Speck, S. P. DenBaars, and S. Nakamura, Appl. Phys. Lett. **103**, 151112 (2013).
[10]A. Pourhashemi, R. M. Farrell, D. A. Cohen, J. S. Speck, S. P. DenBaars, and S. Nakamura, Appl. Phys. Lett. **106**, 111105 (2015).
[11]D. L. Becerra, L. Y. Kuritzky, J. Nedy, A. S. Abbas, A. Pourhashemi, R. M. Farrell, D. A. Cohen, S. P. Denbaars, J. S. Speck, and S. Nakamura, Appl. Phys. Lett. **108**, 091106 (2016).
[12]B. P. Yonkee, E. C. Young, C. Lee, J. T. Leonard, P. Steven, J. S. Speck, and S. Nakamura, Opt. Express **24**, 7816 (2016).
[13]W. G. Scheibenzuber, U. T. Schwarz, R. G. Veprek, B. Witzigmann, and A. Hangleiter, Phys. Rev. B: Condens. Matter Mater. Phys. **80**, 115320 (2009).
[14]S.-H. Park and D. Ahn, Proc. SPIE **8625**, 862511 (2013).
[15]L. Y. Kuritzky and J. S. Speck, MRS Commun. **5**, 463 (2015).
[16]D. C. O'Brien, L. Zeng, H. Le-Minh, G. Faulkner, J. W. Walewski, and S. Randel, in *IEEE International Symposium on Personal, Indoor and Mobile Radio Communications. PIMRC* (2008), p. 1.
[17]H. Le Minh, D. O'Brien, G. Faulkner, L. Zeng, K. Lee, D. Jung, Y. Oh, and E. T. Won, IEEE Photonics Technol. Lett. **21**, 1063 (2009).
[18]C. Lee, C. Zhang, M. Cantore, R. M. Farrell, S. H. Oh, T. Margalith, J. S. Speck, S. Nakamura, J. E. Bowers, and S. P. DenBaars, Opt. Express **23**, 16232 (2015).
[19]C. Lee, C. Shen, H. M. Oubei, M. Cantore, B. Janjua, T. K. Ng, R. M. Farrell, M. M. El-Desouki, J. S. Speck, S. Nakamura, B. S. Ooi, and S. P. DenBaars, Opt. Express **23**, 29779 (2015).
[20]Y. Chi, D. Hsieh, C. Tsai, H. Chen, H. Kuo, and G. Lin, Opt. Express **23**, 13051 (2015).
[21]H. Chun, S. Rajbhandari, D. Tsonev, G. Faulkner, H. Haas, and D. O'Brien, in *Proceedings of the IEEE International Conference on Communication Workshop* (2015), p. 1392.
[22]Y. Chi, D. Hsieh, C. Lin, H. Chen, C. Huang, J. He, B. Ooi, S. P. Denbaars, S. Nakamura, H. Kuo, and G. Lin, Sci. Rep. **5**, 18690 (2015).
[23]B. Janjua, H. M. Oubei, J. R. D. Retamal, T. K. Ng, C.-T. Tsai, H.-Y. Wang, Y.-C. Chi, H.-C. Kuo, G.-R. Lin, J.-H. He, and B. S. Ooi, Opt. Express **23**, 18746 (2015).
[24]C. Shen, T. K. Ng, J. T. Leonard, A. Pourhashemi, H. M. Oubei, M. S. Alias, S. Nakamura, S. P. Denbaars, J. S. Speck, A. Y. Alyamani, M. M. Eldesouki, and B. S. Ooi, ACS Photonics **3**, 262 (2016).
[25]J. C. Carrano, T. Li, C. J. Eiting, R. D. Dupuis, and J. C. Campbell, J. Electron. Mater. **28**, 325 (1999).
[26]R. M. Farrell, C. J. Neufeld, S. C. Cruz, J. R. Lang, M. Iza, S. Keller, S. Nakamura, S. P. Denbaars, U. K. Mishra, and J. S. Speck, Appl. Phys. Lett. **98**, 201107 (2011).
[27]J. R. Lang, N. G. Young, R. M. Farrell, Y. Wu, and J. S. Speck, Appl. Phys. Lett. **101**, 181105 (2012).
[28]B. P. Yonkee, R. M. Farrell, J. T. Leonard, S. P. DenBaars, J. S. Speck, and S. Nakamura, Semicond. Sci. Technol. **30**, 075007 (2015).
[29]FIMMWAVE software package, Photon Design, Ltd., http://www.photond.com/products/fimmwave.htm.
[30]L. Y. Kuritzky, D. L. Becerra, A. S. Abbas, J. Nedy, S. Nakamura, S. P. DenBaars, and D. A. Cohen, Semicond. Sci. Technol. **31**, 075008 (2016).
[31]L. A. Coldren, S. W. Corzine, and M. L. Mašanović, *Diode Lasers and Photonic Integrated Circuits* (John Wiley & Sons, Inc., Hoboken, NJ, USA, 2012).

[32]J. E. Bowers and C. A. Burrus, Jr., J. Light. Technol. **5**, 1339 (1987).
[33]H. Wang, M. Kumagai, T. Tawara, T. Nishida, T. Akasaka, N. Kobayashi, and T. Nishida, Appl. Phys. Lett. **81**, 4703 (2002).
[34]M. Funato, Y. Seok, K. Yoshiaki, O. Akio, K. Yoichi, K. Takashi, and M. S. Nagahama, Appl. Phys. Express **6**, 122704 (2013).
[35]A. Banerjee, T. Frost, E. Stark, and P. Bhattacharya, Appl. Phys. Lett. **101**, 041108 (2012).
[36]T. Frost, A. Banerjee, and P. Bhattacharya, Appl. Phys. Lett. **103**, 211111 (2013).
[37]T. Frost, S. Jahangir, E. Stark, S. Deshpande, A. Hazari, C. Zhao, B. S. Ooi, and P. Bhattacharya, Nano Lett. **14**, 4535 (2014).
[38]T. Melo, Y.-L. Hu, C. Weisbuch, M. C. Schmidt, A. David, B. Ellis, C. Poblenz, Y.-D. Lin, M. R. Krames, and J. W. Raring, Semicond. Sci. Technol. **27**, 024015 (2012).
[39]H. Zhao, R. A. Arif, Y. K. Ee, and N. Tansu, Opt. Quantum Electron. **40**, 301 (2008).
[40]J. E. Bowers, Solid State Electron. **30**, 1 (1987).